

Evolution of the Impurity Band to Diamond-Like Valence Bands in Boron Doped Diamond

Takashi Inushima^{1*}, Yuichi Ota^{1,2}, and Hiromu Shiomi³

¹Department of Electronics, Tokai University, Hiratsuka, Kanagawa 259-1292, Japan

²Tokyo Metropolitan Industrial Technology Research Institute, Koto, Tokyo 135-0064, Japan

³Sumitomo Electric Industries, Ltd., Itami, Hyogo 664-0016, Japan

(Received September 19, 2013; accepted December 18, 2013; published online January 30, 2014)

We present the absorption coefficient and the refractive index of boron doped diamond having an impurity band at 0.07 eV above the valence band maximum and compare them with those obtained by first principles calculation using a C₆₃B supercell model containing 1.57% boron. These optical constants are in good accordance with each other, indicating that the impurity band that forms at *2p* excited states of impurity boron becomes top of the valence bands in metallic condition. Based on this result we present a model of the evolution of boron atoms from isolated impurity to constituent atoms in the boron doped diamond, where the valence electrons of boron become to have *k* dependence and form the top of the valence bands of the C₆₃B supercell diamond.

1. Introduction

Since the discovery of superconductivity in boron-doped diamond,¹⁾ the distribution of impurity boron in diamond has been a key issue for the understanding not only of superconductivity but also of the physics of heavily doped semiconductors. The physical properties of lightly doped diamond are well understood by effective mass approximation.²⁾ When the doping concentration N_B exceeds a critical value of $N_c \sim 3 \times 10^{20} \text{ cm}^{-3}$, Mott transition occurs and the diamond becomes a metal.³⁾ It is understood that when a carrier concentration of a semiconductor is close to N_c , the carriers are scattered by defects and the mean free path becomes shorter, and finally Anderson localization is established.⁴⁾ Actually the superconducting diamond is close to the localization limit of $k_F l \simeq 1$ (k_F is the Fermi wavenumber and l is the carrier mean free path).⁵⁾

However, a study by an angle-resolved photoemission spectroscopy (ARPES) revealed that the superconducting diamond had clear solid diamond valence bands and its Fermi energy shifted according to the increase of doping density.⁶⁾ This result is understood to show that the impurity states are absent or located above the Fermi level.⁷⁾ Interesting enough, the observed bands are reproduced well by a supercell-model calculation where boron is a constituent atom.^{8,9)} On the other hand, Shirakawa et al. claimed that boron should be randomly distributed in diamond and form a disordered potential.¹⁰⁾ They questioned the supercell model which could not explain the continuous evolution of the impurity states according to the increase of N_B ; from the separate level to the rigid band shift of the Fermi energy in the valence band. But it should be stressed that the impurity band concept applied in conventional semiconductors like Si and Ge does not work in diamond.¹¹⁾

In our previous papers we reported that when N_B exceeds $\sim 4 \times 10^{18} \text{ cm}^{-3}$, the *2p* wave functions of impurity boron begin to overlap, and an impurity band forms not at the *1s* ground level but at the *2p* excited states, which is located ~ 0.07 eV above the valence band maximum. Simultaneously, the Fermi level rises to this impurity band and the relaxation time of the excited holes decreases drastically.^{12,13)} Takeuchi et al. obtained similar results of the impurity band structure

with the carrier concentration close to and below N_c using a total photoelectron emission yield spectroscopy.¹⁴⁾ This is a remarkable feature of diamond and it is important to understand how the impurity band evolves into solid bands in boron doped diamond.

In this paper, we present the absorption coefficient and the refractive index of boron doped diamond with an impurity band, and show that they are in good accordance with those obtained by first principles calculation using a supercell model of C₆₃B. Then we develop the idea presented in our previous works and show the boron concentration dependence of the Fermi level, and the impurity band evolution caused by hybridization of boron atoms and carbon atoms.

2. Experimental Details

The home-epitaxial films used in the experiments were grown by the microwave-enhanced chemical vapor deposition method on an off-oriented Ib synthesized diamond surface, which was (001) with 7° off-angle toward (100). H₂ and CH₄ were used as source gases with a ratio of CH₄/H₂ of 2%. B₂H₆ (10 ppm diluted by H₂) was used as a doping gas. The ratio of B/C in the reaction gas phase was used to identify the samples, which was twice the value of that used in the previous papers, where the ratio of B₂H₆/CH₄ was used.^{15–17)} The boron concentration determined by a secondary ion mass spectroscopy was 1 to $10 \times 10^{19} \text{ cm}^{-3}$ in the 10,000 ppm B/C sample.¹⁸⁾ The boron-doped layer thickness was 1.6 μm. There was a clear change of conductivity from the valence band to the variable range hopping (VRH) when $N_B \simeq 4 \times 10^{18} \text{ cm}^{-3}$.¹⁶⁾ From the conductivity and Hall measurements, the B/C = 10,000 ppm sample had $N_B = 2 \times 10^{19} \text{ cm}^{-3}$,¹²⁾ which was one order of magnitude smaller than N_c .

Temperature dependence of the absorption and reflection spectra was measured using a synchrotron beam at UVSOR II of Institute for Molecular Science. In the infrared region BL-6B was used together with a DTGS detector.¹⁹⁾ In visible and UV regions the reflection spectrum was obtained by BL-7B, where a 3 m focal length Perkin-Elmer monochromator and a silicon photodiode were employed at 8° to the normal incident configuration. The resolution was 0.3 meV at 4 eV.

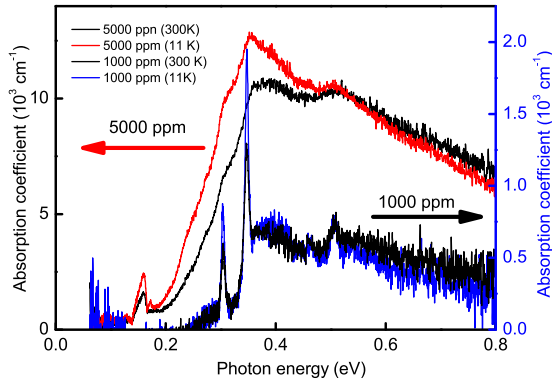


Fig. 1. (Color online) Temperature dependence of the absorption spectra of boron doped diamond with (B/C = 5000 ppm) and without (B/C = 1000 ppm) an impurity band.

3. Experimental Results

3.1 Temperature dependence of the boron induced absorption

Figure 1 shows a comparison of the temperature dependence of the absorption spectra of boron doped diamond with and without an impurity band. The spectra of the B/C = 1000 ppm sample have isolated sharp Gaussian shape absorptions at 0.305 and 0.347 eV, which are the carrier transitions from the boron 1s ground state to the first and the second 2p excited states, respectively.^{11,20)} When the temperature decreases, the peaks become sharper and the intensity almost doubles. However, the phonon sidebands observed at 0.46 and 0.51 eV, and the band continuum at 0.37 eV do not show any temperature dependence. The temperature dependence of the peak intensity and the broadening is explained by the temperature dependence of the lifetime due to acoustic phonon interactions.¹¹⁾

When an impurity band exists as in the B/C = 5000 ppm sample, the absorption spectrum has a Lorentzian shape governed by the single absorption at 0.35 eV, and fine structure is not observed. This is because the Fermi level rises to the 2p excited states and the relaxation time of the excited carriers decreases drastically.¹³⁾ As the temperature decreases, the absorption coefficient at the peak increases by 20% and a shoulder at ~0.3 eV becomes obvious, which is caused by the increase of the absorption component at 0.305 eV. Such weak temperature dependence of the absorption spectra suggests that despite some boron remaining as isolated impurity, most boron forms the impurity band.

The shape of the absorption spectra observed at ~0.16 eV in Fig. 1 is almost the same as what was assigned as defect-induced-first-order (DIFO) phonon absorption.^{2,11)} However, the reported DIFO absorption coefficient is ~1 cm⁻¹, and it is difficult to detect it in our sample thickness. Moreover, as is seen in the B/C = 5000 ppm sample, when the sample has an impurity band, DIFO absorption coefficient becomes larger than 1000 cm⁻¹ and depends strongly on temperature.

Figure 2 shows detailed DIFO absorption spectra at 11 K of three samples with an impurity band. Though the DIFO spectrum shows a one-phonon excitation of the bulk diamond in the Brillouin zone, the absorption coefficient at 0.16 eV is proportional to the boron concentration. It is reported that due to a partial loss of translational symmetry, the DIFO spectrum contains a sharp absorption peak at the Raman active optical

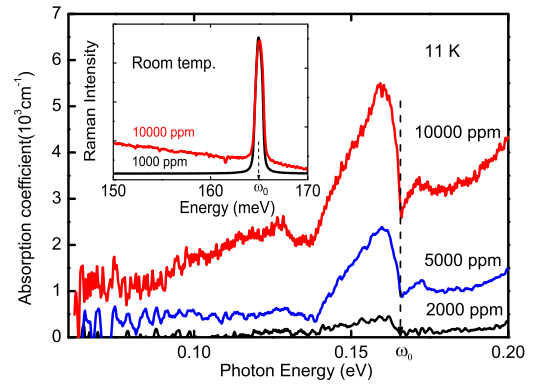


Fig. 2. (Color online) Temperature dependence of the absorption spectra of boron doped diamond with an impurity band. Inset shows the micro-Raman spectra of the B/C = 10,000 and 1000 ppm samples obtained using 633 nm excitation energy under backscattering configuration at room temperature. ω_0 is the Raman active phonon energy.

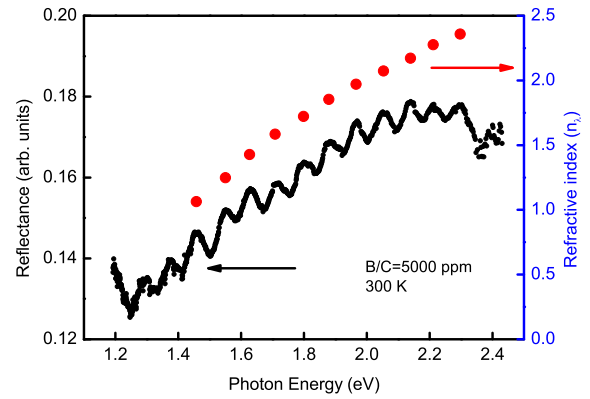


Fig. 3. (Color online) Reflection spectra of the B/C = 5000 ppm diamond sample. The n_r is plotted using Eq. (1).

phonon energy of $\omega_0 = 0.165$ eV.²⁾ However, this phonon energy corresponds to the upper sharp cut-off of the DIFO absorption in Fig. 2.

A strong disorder induced broadening of the optical phonon of heavily boron-doped diamond is reported in the Raman spectra.²¹⁾ However, as is shown in the inset of Fig. 2, the micro-Raman spectrum of the optical phonon of the investigated samples does not show any disorder induced broadening. Hence we conclude that the absorption shown in Fig. 2 has not been induced by the defect, but that it has become infra-red active absorption because of the occurrence of the impurity band.

3.2 Refractive index of the impurity band

As measuring the refractive index by an ellipsometry is complex, we measured them using the reflection spectrum, which is shown in Fig. 3 for the B/C = 5000 ppm sample. Sinusoidal oscillation is observed in the energy range from 1.2 to 2.4 eV. In other energy region there is no structure. For a nearly non-absorbing boron doped diamond film with a refractive index n_f on a diamond substrate with index n_s , the reflectivity R at normal incidence is expressed as follows;

$$R = \frac{r_{10}^2 + r_{21}^2 + 2r_{10}r_{21} \cos \gamma}{1 + r_{10}^2 r_{21}^2 + 2r_{10}r_{21} \cos \gamma}, \quad (1)$$

where, $r_{10} = (1 - n_\lambda)/(1 + n_\lambda)$ and $r_{21} = (n_\lambda - n_s)/(n_\lambda + n_s)$ are the Fresnel coefficients between air and the film, and the film and the substrate, respectively. $\gamma = 4\pi dn_\lambda/\lambda$ is the optical path difference at wavelength λ , and d is the film thickness. When $n_\lambda \geq 1$, the maxima in the fringe corresponds to $\gamma = 2\pi m$, where m is an integer.

To estimate n_λ using Eq. (1), the absolute value of m is chosen so as to fit n_λ below the bulk diamond value of $n_s = 2.46$. Then we set $m = 3$ at the maxima of the fringe at ~ 1.5 eV, where n_λ exceeds 1. Thus n_λ in Fig. 3 is obtained using the positions indicated in the figure. The estimated n_λ gives $R \sim 0.15$ in the investigated region.

In the energy region below 1.5 eV where the signal is weak and noisy, the contribution of the absorption is important and Eq. (1) is not applicable. Bustarret et al. reported on the refractive index of a $1.2 \times 10^{21} \text{ cm}^{-3}$ boron doped diamond.²¹⁾ They presented a concave dependence of the refractive index against energy, from 1.7 at 1 eV to 2.5 at 5 eV, which is similar to the energy dependence shown in Fig. 3.

4. First Principles Calculation

The electronic structure and the dielectric constants of 1.57% boron doped diamond ($C_{63}B$) were calculated by first principles technique. We employed a super-cell model, a 64-atom supercell constructed of $2 \times 2 \times 2$ simple cubic 8-atom cells. One carbon atom was substituted by one boron atom. The lattice parameters were determined so as to minimize the total energy of the crystal, and the obtained lattice constant was 3.546 \AA , which was in good agreement with 3.567 \AA of typical diamond. We employed the density functional theory (DFT) provided in the code ADVANCE/PHASE.²²⁾ Ultrasoft pseudopotentials were used, with the Perdew–Burke–Ernzerhof (PBE) generalized gradient approximation for the exchange–correlation functional. The plane-wave basis set with a 25 hartree cutoff energy was taken and a mesh of $8 \times 8 \times 8$ Monkhorst–Pack k -points sampling was used for the integration of the Brillouin zone.

Electronic dielectric function ϵ_2 was calculated using a position operator r as follows;

$$\epsilon_2 = \frac{e^2}{\pi^2} \sum_{c,v} \int |\langle \Psi_c(k) | u \cdot r | \Psi_v(k) \rangle|^2 \delta(E_c^k - E_v^k - \hbar\omega) dk, \quad (2)$$

where u is the polarization vector of the incident light, $\hbar\omega$ is the energy difference between the conduction (c) and valence (v) bands, E_c^k and E_v^k represent the Kohn–Sham energy level of the band at the wave vector k obtained using wave functions $\Psi_c(k)$ and $\Psi_v(k)$. The integration was done by Linear-Tetrahedron method,²³⁾ and the summation was made for all the combinations of v and c . The transition moments were corrected using the method of Kageshima and Shiraishi.²⁴⁾

The real part ϵ_1 was calculated from the ϵ_2 using the Kramers–Kronig relation, and with the combination of ϵ_1 and ϵ_2 , we obtained the refractive index n_λ . Figure 4 shows the n_λ of $C_{63}B$ together with that of the supercell C_{64} calculated using the same parameters. There is a strong anomalous dispersion at ~ 0.5 eV caused by boron impurity, which is the major difference of n_λ between C_{64} and $C_{63}B$ as is shown in the inset of Fig. 4. Due to this anomalous dispersion, the calculated n_λ is smaller than 2.46, which is what is observed in the bulk diamond and C_{64} below 2.5 eV. n_λ becomes smaller than 1 below 0.8 eV, and has a convex dependence on

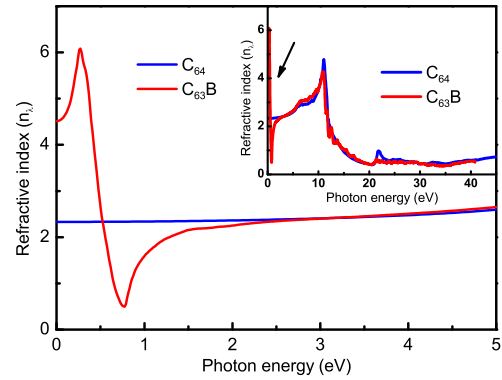


Fig. 4. (Color online) Comparison of the refractive index (n_λ) of intrinsic (C_{64}) and 1.57% boron doped ($C_{63}B$) diamonds. The inset shows the comparison of the n_λ in the total energy range, where the main panel region is indicated by an arrow.

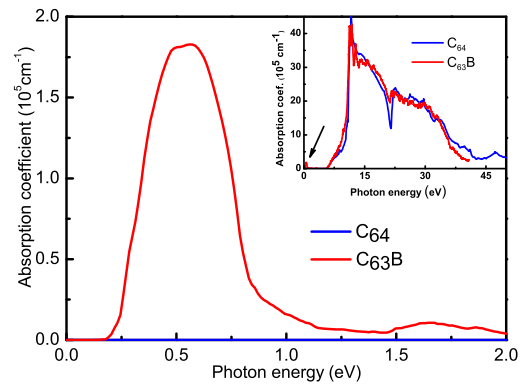


Fig. 5. (Color online) Comparison of the absorption coefficient of intrinsic (C_{64}) and 1.57% boron doped ($C_{63}B$) diamonds. The inset shows the comparison in the total energy range, where the main panel region is indicated by an arrow.

the increase of energy, which is in accordance with what we have observed in Fig. 3.

The absorption coefficient is calculated using ϵ_1 and ϵ_2 , which is shown in Fig. 5. There is a sharp and strong absorption of $1.7 \times 10^5 \text{ cm}^{-1}$ at ~ 0.5 eV, which is one order of magnitude larger than that shown in Fig. 1. Electrically determined boron concentration of the B/C = 5,000 ppm sample is two orders of magnitude smaller than that of $C_{63}B$.

As is shown in the inset of Fig. 5, the absorption induced by boron is observed at 0.5 eV above the valence band maximum (VBM) as a separate peak. This is because the threefold degeneracy of the VBM is held in this calculation. Detailed VBM of $C_{63}B$ is shown in Fig. 6(A). The band has a hole pocket and the Fermi level is 0.18 eV below the VBM. The bands labeled a , b , and c are not split at Γ point because of the symmetry, and there are threefold degenerate bands d , e , and f , which newly appear due to the boron involvement. These features are similar to those of the $C_{127}B$ supercell model calculated by Lee and Pickett.⁹⁾

The bands that contribute to the absorption at 0.5 eV are determined by computing the separate absorption coefficients. They are calculated using Eq. (2) and shown in Fig. 6(B), where the initial valence and the final conduction bands are specified in the legends. Since the absorption coefficient shown in Fig. 6(B) is calculated without taking the combinations of c and v in Eq. (2), there is a small

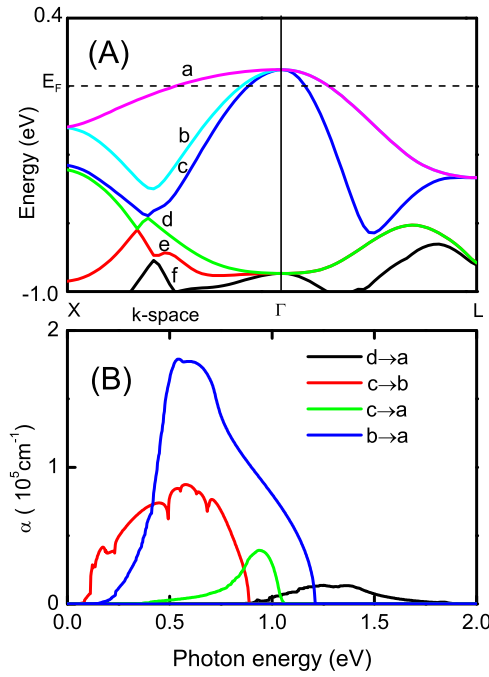


Fig. 6. (Color online) (A) Valence band structure of the $C_{63}B$ supercell. (B) Absorption coefficients of the optical transitions between the bands labeled in (A). The transition direction is indicated by the arrows in the legend.

discrepancy between the sum of the separately calculated absorption coefficients and that shown in Fig. 5. However it is obvious that the absorption is caused by $b \rightarrow a$ and $c \rightarrow b$ transitions, which are the intraband transitions between the topmost valence bands of $C_{63}B$.

Periodicity of boron atoms is absent in the diamond where the boron impurities are randomly distributed. Focusing on this point, Lee and Pickett studied the band structure of metallic diamond calculated using a supercell model and coherent potential approximation (CPA), and concluded that the CPA and supercell results were similar at the valence band structure near the Fermi level.⁹⁾ Hence it is expected that the metallic boron-doped diamond has a sharp and strong intraband absorption, which causes the big change of the refractive index shown in Fig. 4.

5. Discussion

When we compare the optical constants of the boron doped diamond with an impurity band and those of a $C_{63}B$ supercell obtained by the first principles calculation, it is obvious that the calculated values will be experimentally obtained at one order of magnitude larger N_B . In other words, a boron doped diamond with an impurity band is in a C_xB supercell condition. That is, when the N_B is small, boron has a separated energy level expressed by the Bloch wavefunctions of the valence band maxima. However, when the $2p$ wavefunctions of impurity boron begin to overlap at $N_{c1} = 4 \times 10^{18} \text{ cm}^{-3}$ ($B/C = 2000 \text{ ppm}$), an impurity band appears at the $2p$ excited level. Simultaneously, the Fermi energy shifts to the $2p$ excited level, which indicates that the diamond with the impurity band has a metallic character. Then, the topmost valence band structure is determined by the valence electrons of boron as is expected in the supercell condition, and the separate impurity states fade into the valence band.

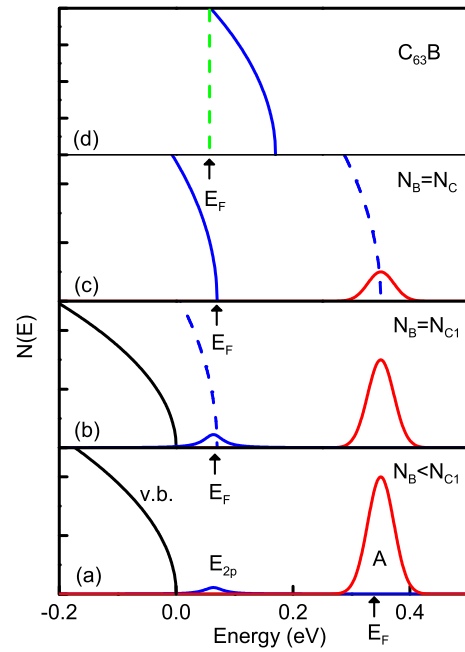


Fig. 7. (Color online) Boron concentration (N_B) dependence of the impurity band structure in diamond. Band A forms at the boron ground states. E_F is the Fermi level position. N_{c1} is the critical density for the change of the conduction. N_c is the Mott transition density. The dashed lines are the density of states formed by boron wave functions.

The infra-red active phonon density of states in the 0.15 eV region induced by the impurity band shown in Fig. 2 is another evidence of the C_xB supercell condition. The phonon structure of the boron doped diamond was calculated using a supercell model, and because of the boron involvement, phonon softening, which plays an important role for the occurrence of the superconductivity, is expected at the highest frequency of the zone center optical phonons.²⁵⁾ Actually the phonon softening was experimentally observed in superconducting diamond.²⁶⁾ Moreover, the observed softening was much closer to that expected by supercell model calculation than that by virtual crystal approximation.²⁷⁾ These results offer a scenario where the boron atoms are involved in the carbon network, satisfying the C_xB supercell condition.

In previous papers we showed how boron impurity evolved from isolated level to an impurity band.^{12,13)} Now, the first principles calculation shows that the impurity band continues to evolve into the solid valence band through Mott transition. Here, we present an idea of the evolution, schematically shown in Fig. 7.

When N_B is small, boron has the energy level at A, which is 0.37 eV above the valence band maximum, and the $2p$ excited level is isolated, which is shown in Fig. 7(a). The Fermi level depends on the degree of compensation. When N_B is larger than the number of charged donors, the Fermi level lies in band A (E_F). When the temperature is high, conduction is governed by the carriers excited from the Fermi level to the valence band maximum.

The conduction mechanism drastically changes at N_{c1} , which is shown in Fig. 7(b). At N_{c1} the average distance between borons is $\approx 4 \text{ nm}$, and the $2p$ wavefunction starts to overlap that of the neighboring boron atoms, and E_F rises to the E_{2p} position.¹³⁾ Hence, the supercell condition is partially

satisfied and the $2p$ wavefunctions have k dependence. The appearance of k dependence is indicated by the dashed line.

In our model Mott transition occurs when the Fermi level reaches the top of the valence band at $N_B = N_c$ ($\sim 3 \times 10^{20} \text{ cm}^{-3}$), which is shown in Fig. 7(c). The impurity band formed by $2p$ wavefunctions merges into the bulk diamond band at N_c . The energy position of the top of the valence band is not the same as that of the intrinsic one and it should be determined by the supercell condition. At N_c , the $1s$ wave functions of borons partially overlap and have k dependence, but the majority remains in isolated condition. Hence, the absorption spectrum is governed by the transition between A and the top of the valence band.

Figure 7(d) corresponds to the $C_{63}B$ supercell condition and $E_F = -0.18 \text{ eV}$. From a study by an X-ray absorption and emission spectroscopy, it is reported that there is an in-gap state about 0.3 eV above the top of the valence band in the metallic and nonmetallic boron doped diamonds.²⁸⁾ We understand that the in-gap state is, when N_B is 0.1% , the impurity band absorption shown in Fig. 1, and when N_B is 4.3% , it is the intra-band absorption shown in Fig. 5. This assignment supports the idea of the impurity band structure presented in Fig. 7. Moreover, the band structure of the $C_{63}B$ supercell is almost the same as that of bulk diamond, which explains the result given by a photoemission spectroscopy.⁶⁾ In Figs. 7(a) to 7(d) there is no drastic change of the absorption spectra, because the transition including the intra-band transition is governed mainly by boron wavefunctions.

In usual semiconductor physics, heavily doped impurity disturbs the crystal ordering and the potential fluctuation induces Anderson localization.⁴⁾ This scenario does not work in the superconductivity of diamond. Experimentally, it is reported from a nuclear magnetic resonance study of superconducting diamond that, though boron is distributed randomly in diamond, the boron that substitutes carbon in the high symmetry diamond structure produces effective carriers for the superconductivity, while the boron in the lower local symmetry does not.²⁹⁾ This result supports our model where the doped boron works as a constituent atom in the bulk having a C_xB supercell and the potential disturbance is not so strong. Moreover, the involvement of boron atoms in diamond structure is advantageous to producing a strong bond polarization and inducing a strong electron–phonon interaction as has been observed in the superconductivity of semiconductor InN which also shows superconductivity near the Mott transition.³⁰⁾

6. Summary

We compared the absorption coefficient and the refractive index of boron doped diamond having an impurity band at 0.07 eV above the valence band maximum and those obtained by first principles calculation using a $C_{63}B$ supercell model containing 1.57% boron. From the comparison we presented a model of the evolution of boron atoms from isolated impurity to constituent atoms in the boron doped diamond, where, when the boron concentration exceeds $4 \times 10^{18} \text{ cm}^{-3}$, the valence electrons of boron become to have k dependence, and they form the top of the valence bands of $C_{63}B$ supercell diamond. The presented model explains the boron concentration dependence of the reported X-ray absorption and emission spectra.

Acknowledgments

This work was supported by the Joint Studies Program (2011) of the Institute for Molecular Science. The authors are grateful to the Ministry of Education, Culture, Sports, Science and Technology of Japan for the Grant-in-Aid for Scientific Research No. 22560304.

*inushima@keyaki.cc.u-tokai.ac.jp

- 1) E. A. Ekimov, V. A. Sidorov, E. D. Bauer, N. N. Mel'nik, N. J. Curro, J. D. Thompson, and S. M. Stishov, *Nature* **428**, 542 (2004).
- 2) H. Kim, R. Vogelgesang, A. K. Ramdas, S. Rodriguez, M. Grimsditch, and T. R. Anthony, *Phys. Rev. B* **57**, 15315 (1998).
- 3) Y. Takano, M. Nagao, T. Takenouchi, H. Umezawa, I. Sakaguchi, M. Tachiki, and H. Kawarada, *Diamond Relat. Mater.* **14**, 1936 (2005).
- 4) B. I. Shklovskii and A. L. Efros, *Electronic Properties of Doped Semiconductors* (Springer, Heidelberg, 1984).
- 5) K. Ishizaka, R. Eguchi, S. Tsuda, A. Chainani, T. Yokoya, T. Kiss, T. Shimojima, T. Togashi, S. Watanabe, C.-T. Chen, Y. Takano, M. Nagao, I. Sakaguchi, T. Takenouchi, H. Kawarada, and S. Shin, *Phys. Rev. Lett.* **100**, 166402 (2008).
- 6) T. Yokoya, T. Nakamura, T. Matsushita, T. Muro, Y. Takano, M. Nagao, T. Takenouchi, H. Kawarada, and T. Oguchi, *Nature* **438**, 647 (2005).
- 7) H. Okazaki, T. Yokoya, J. Nakamura, N. Yamada, T. Nakamura, T. Muro, Y. Tamenori, T. Matsushita, Y. Takata, T. Tokushima, S. Shin, Y. Takano, M. Nagao, T. Takenouchi, H. Kawarada, and T. Oguchi, *J. Phys. Chem. Solids* **69**, 2978 (2008).
- 8) X. Blase, Ch. Adessi, and D. Connétable, *Phys. Rev. Lett.* **93**, 237004 (2004).
- 9) K.-W. Lee and W. E. Pickett, *Phys. Rev. B* **73**, 075105 (2006).
- 10) T. Shirakawa, S. Horiuchi, Y. Ohta, and H. Fukuyama, *J. Phys. Soc. Jpn.* **76**, 014711 (2007).
- 11) S. D. Smith and W. Taylor, *Proc. Phys. Soc.* **79**, 1142 (1962).
- 12) R. F. Mamin and T. Inushima, *Phys. Rev. B* **63**, 033201 (2001).
- 13) T. Inushima, R. F. Mamin, and H. Shiomi, *Phys. Rev. B* **79**, 045210 (2009).
- 14) D. Takeuchi, M. Ogura, N. Tokuda, H. Okushi, and S. Yamasaki, *Phys. Status Solidi A* **206**, 1991 (2009).
- 15) A. Ogasawara, T. Inushima, T. Shiraishi, S. Ohya, S. Karasawa, and H. Shiomi, *Diamond Relat. Mater.* **6**, 835 (1997).
- 16) T. Inushima, A. Ogasawara, T. Shiraishi, S. Ohya, S. Karasawa, and H. Shiomi, *Diamond Relat. Mater.* **7**, 874 (1998).
- 17) T. Inushima, T. Matsushita, S. Ohya, and H. Shiomi, *Diamond Relat. Mater.* **9**, 1066 (2000).
- 18) H. Shiomi, Y. Nishibayashi, N. Toda, and S. Shikata, *IEEE Electron Device Lett.* **16**, 36 (1995).
- 19) S. Kimura, E. Nakamura, T. Nishi, Y. Sakurai, K. Hayashi, J. Yamazaki, and M. Katoh, *Infrared Phys. Technol.* **49**, 147 (2006).
- 20) M. I. Eremets, *Semicond. Sci. Technol.* **6**, 439 (1991).
- 21) E. Bustarret, E. Gheeraert, and K. Watanabe, *Phys. Status Solidi A* **199**, 9 (2003).
- 22) Web [http://www.advancesoft.jp/product/advance_phase/].
- 23) G. Lehmann and M. Taut, *Phys. Status Solidi B* **54**, 469 (1972).
- 24) H. Kageshima and K. Shiraishi, *Phys. Rev. B* **56**, 14985 (1997).
- 25) H. J. Xiang, Z. Li, J. Yang, J. G. Hou, and Q. Zhu, *Phys. Rev. B* **70**, 212504 (2004).
- 26) M. Hoesch, T. Fukuda, J. Mizuki, T. Takenouchi, H. Kawarada, J. P. Sutter, S. Tsutsui, A. Q. R. Baron, M. Nagao, and Y. Takano, *Phys. Rev. B* **75**, 14058(R) (2007).
- 27) L. Boeri, J. Kortus, and O. K. Andersen, *Phys. Rev. Lett.* **93**, 237002 (2004).
- 28) J. Nakamura, N. Yamada, K. Kuroki, T. Oguchi, K. Okada, Y. Takano, M. Nagao, I. Sakaguchi, T. Takenouchi, H. Kawarada, R. C. C. Perera, and D. L. Ederer, *J. Phys. Soc. Jpn.* **77**, 054711 (2008).
- 29) H. Mukuda, T. Tsuchida, A. Harada, Y. Kitaoka, T. Takenouchi, Y. Takano, M. Nagao, I. Sakaguchi, T. Oguchi, and H. Kawarada, *Phys. Rev. B* **75**, 033301 (2007).
- 30) T. Inushima, D. K. Maude, H. Lu, W. J. Schaff, T. Iizuka, S. Kimura, A. Yamamoto, and K. Fukui, *J. Phys. Soc. Jpn.* **81**, 044704 (2012).